Maximizing Alq_3 OLED Internal and External Efficiencies: Charge Balanced Device Structure and Color Conversion Outcoupling Lenses

Weixin Li, *Student Member, IEEE*, Robert A. Jones, *Student Member, IEEE*,
Steven C. Allen, *Student Member, IEEE*, Jason C. Heikenfeld, *Member, IEEE*, and
Andrew J. Steckl, *Fellow, IEEE*

***Abstract*—In this paper, we report bright, efficient Alq_3-based [tris-(8-hydroxyquinoline) aluminum] organic light-emitting diode (OLED) structures that incorporate hemispherical lenses for increased output power efficiency. The 6-layer hybrid (polymer/small molecule) OLED structure contains two spin-coated polymer layers and four thermally evaporated small molecule layers. This structure results in balanced charge injection, thus leading to a more efficient device. The use of index-matched transparent lenses resulted in luminous and external quantum efficiency of 7.5 lm/W and 8%, respectively. The size and shape of the lens was used to control the angular power distribution. Lenses incorporating color conversion media were used to achieve high OLED efficiency in various colors. Saturated yellow, orange, and red devices with external quantum efficiencies as high ~4% were obtained from this approach.**

***Index Terms*—Alq_3, color conversion efficiency, color conversion material, lensed device, luminous intensity, organic light emitting diodes (OLED), outcoupling efficiency, quantum efficiency.**

I. INTRODUCTION

ORGANIC light-emitting devices (OLEDs), using Alq_3 (tris(8-hydroxyquinoline) aluminum) as both electron transport material (ETM) and emitter layer, have attracted great interest since Tang and Van Slyke [1] reported their first bilayer device in 1987. OLEDs are being extensively investigated and are beginning to be commercially utilized in electronic display and solid-state lighting applications [2]–[4].

In order to obtain more balanced charge injection from both the anode and cathode, multilayer OLED devices are studied intensively so as to lower the device operating voltage and to increase the device luminance and output power efficiency. To achieve this end, one approach is to enhance electron injection at the cathode/ETM interface by: 1) using low work function metals [5]–[8] and 2) introducing a thin layer of electron injection material with high electron affinity between the cathode and ETM in order to increase electron injection through stepwise injection from the cathode [9], [10]. A second approach is to increase the hole injection by using: 1) UV-ozone treated indium tin oxide (ITO) [11]; 2) high work function anodes [12]; and 3) a thin layer of hole injection material (HIM) with a lower ionization potential than that of hole transport material (HTM) in order to enhance hole injection [13]–[15] through stepwise injection from the anode.

The imbalance of the electron/hole (e/h) energy barriers in the heterostructure and the differences of e/h mobility should be taken into account during device design [16]. Charge injection balance is an extremely important issue in achieving high efficiency OLED devices. During device operation, unbalanced injection of electrons or holes will result in nonradiative recombination of the charge carrier species at either the organic/cathode or the organic/anode interfaces [17]. In designing a device structure with charge-balanced operation, one needs to consider both the effect of the energy barriers on charge injection and the effect of e/h mobilities on charge transport.

Alq_3 is widely employed as the emissive layer in small molecule OLEDs. Devices with purely Alq_3 material as the emitter layer generally yield an external quantum efficiency $\eta_{\mathrm{ext}} \sim 1\%$ [13], [14], [18], which is still much less than that anticipated [19] from the high photoluminescence (PL) efficiency (~30%) of the material, suggesting a large potential for improvement in these devices if a highly charge balanced device structure can be designed. Additionally, a considerable portion of the light originating from emissive centers never escapes from the device due to total internal reflection when the emitted light exceeds the critical angle at both the device/substrate interface and the substrate/air interface within an OLED. This reflected fraction of the emitted light is finally either dissipated by metal electrode absorption or waveguided within the glass substrate, resulting in edge emission.

The external quantum efficiency, expressed as number of photons emitted into the viewing direction for every electron injected, is given by $\eta_{\mathrm{ext}} = \eta_{int} \times \eta_{\mathrm{oc}} = \gamma \times \eta_s \times \phi_f \times \eta_{\mathrm{oc}}$, where η_{int} is the internal quantum efficiency (i.e., total photons generated per injected electron); η_{oc} is the outcoupling efficiency; γ is the charge carrier balance factor, namely the ratio of electrons/holes at the recombination region; η_s is the efficiency of singlet formation and ϕ_f is the quantum efficiency of fluorescence. η_s and ϕ_f are properties of the selected material. As a result, balancing the charge injection becomes the easiest way to increase the internal efficiency for Alq_3 OLEDs.

The external and internal quantum efficiencies are connected by the device outcoupling efficiency η_{oc}. This factor has been approximately evaluated using a simple ray-optics model [20], [21]. According to the model, more than 80% of produced pho-

---

Manuscript received December 8, 2005; revised February 9, 2006. This work was supported by the University of Cincinnati Institute for Nano Science and Engineering.

The authors are with the Nanoelectronics Laboratory, University of Cincinnati, Cincinnati, OH 45221-0030 USA (e-mail: a.steckl@uc.edu).

Digital Object Identifier 10.1109/JDT.2006.874507

tons are confined within the device and, thus, not available for a useful function.

Several methods have been reported for increasing the outcoupling efficiency. The external outcoupling efficiency can be improved $\sim 2\times$ by etching grooves in the glass around the OLED device in order to redirect light trapped in the glass substrate and organic/ITO layers [21]. η_{ext} can be improved $\sim 1.8\times$ by inserting a low refractive index $(n < 1.03)$ silica aerogel layer between the glass substrate and the ITO layer [22]. An increase in outcoupling efficiency of $\sim 2\times$ can also be achieved by integrating optical elements within the OLED device structure [21], [23], which direct more of the emitted light out of the device.

In this paper, we report a bright, efficient hybrid Alq$_3$ OLED structure with two layers of spin-coated polymers and four layers of thermally evaporated small molecules. The schematic device structure and dimensions are shown in Fig. 1(a) and (b). The polymer materials serve as hole injection and charge balance layers, while small molecule materials are used as electron transport, hole blocking, emitter, and hole transport layers. Enhancements in outcoupling efficiency have been achieved through the use of index-matched transparent hemispherical lenses. Additionally, lenses containing color conversion materials were used to obtain high efficiency at different colors. Saturated yellow, orange, and red devices with high efficiency were obtained from this approach. These high efficiency devices can significantly reduce power consumption, so as to extend the OLED device operational lifetime.

II. EXPERIMENTAL PROCEDURES

The fabrication process starts with sputter deposition of the indium tin oxide (ITO) anode layer on Corning 1737 glass substrates $(n = 1.46)$. The ITO $(\rho = 60\ \Omega/\square,\ n = 1.95)$ is then patterned and cleaned with methanol and acetone ultrasonic bath treatments for 30 minutes each, followed by being thoroughly rinsed in de-ionized water and dried in an oven. Next, two polymer layers of PEDOT [poly(3,4-ethylenedioxythiophene) doped with poly(4-styrenesulfonate)] (Baytron-P from H. C. Stark) and PVK [poly(N-vinylcarbazole)] (Acro Organics) are sequentially spin-coated onto the patterned ITO glass substrate. The aqueous PEDOT solution is diluted, filtered and spin-coated at a speed of 2000 rotations per minute (rpm). The film is then hard baked at 150 °C for 15 min before applying PVK, resulting in a film thickness of ~30 nm. PVK solution (4 mg/ml) is filtered and spin-coated afterward at the same speed. The spin-coated wafer is then rapidly transferred into an ultra high vacuum molecular beam deposition (MBD) system (from SVT Association) and baked under vacuum at 140 °C for 10 min. TPD [N,N′-diphenyl-N,N′-bis(3-methylphenyl)1-1′-biphenyl-4-4′-diamine] or NPB [(N,N′-bis (naphthalene-1-yl)-N,N′-bis(phenyl) benzidine)], Alq$_3$ and BCP [2,9-dimethyl-4,7-diphenyl-1,10-phenanthroline] (all from H. W. Sands) are then thermally evaporated with a deposition rate of $\sim$ 2 Å/s at a base pressure of 10^{-8} torr. LiF is evaporated next, at a rate of 1 Å/s. The wafer is then briefly removed to apply the Al cathode shadow mask. The active device area is $2 \times 2\ \text{mm}^2$. Finally, the substrate is reinserted into the MBD system and Al is evaporated at 7 Å/s.

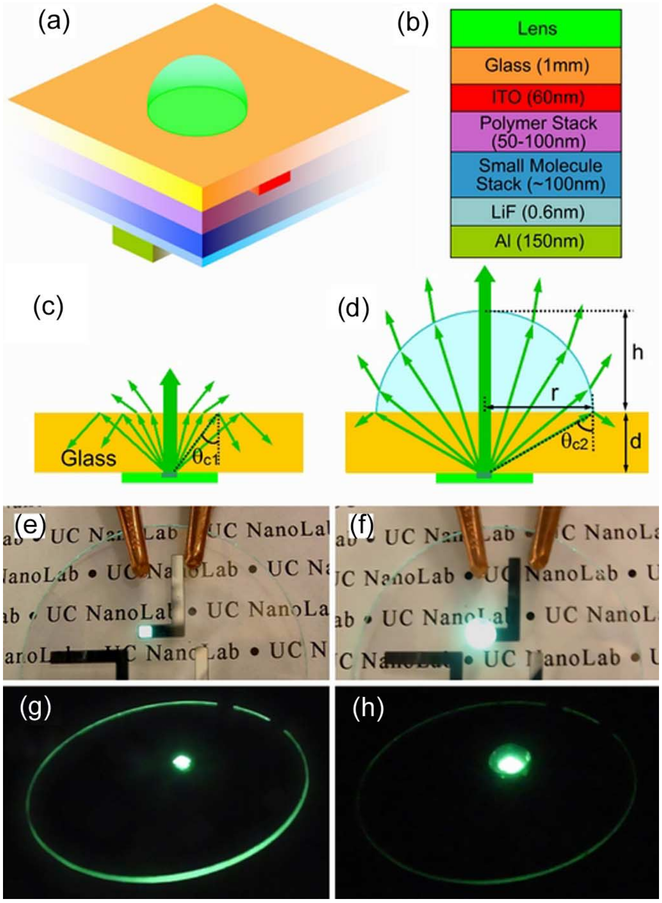

Fig. 1. High outcoupling efficiency of Alq$_3$ OLED using index-matched lenses. (a) Schematic structure of lensed Alq$_3$ device. (b) Cross section of Alq$_3$ device with layer dimensions; (c) light output scheme without lens. (d) Light output scheme with lens. (e) Emission from lensless device operating at 6 V. (f) Emission from device with 2.5-mm lens operating at 6 V. (g) Waveguiding effect for lensless device at 6 V; (h) waveguiding effect for device with 4-mm lens at 6 V. (Color version available online at http://ieeexplore.ieee.org.)

OLEDs are tested at room temperature without any encapsulation. Various transparent epoxy lenses $(n = 1.56)$ with spherical radius of 2.5, 4 and 5 mm, and different dome heights (high: $h = 8$ mm, medium: $h = 5$ mm and low: $h = 3$ mm for the 5-mm-radius lens only) are attached to the glass side of the OLED device with index matching liquid; $n = 1.51$. The refractive indices of the materials in our device are: glass $(n = 1.46)/\text{ITO}(n = 1.95)/\text{PEDOT}(n = 1.51)/\text{PVK}(n \approx 1.7)/\text{TPD}(n = 1.76)/\text{Alq}_3(n = 1.7)/\text{BCP}(n = 1.7)/\text{LiF}(n = 1.39)$.

The color conversion material (CCM) lenses are fabricated by molding mixtures of molten soft silicone gel $(n = 1.4)$ and different CCMs. Three different CCM designs were fabricated for comparison: CCM disk; CCM lens and partially CCM lens (pCL). The lenses are about 4 mm high with a spherical radius of ~3.2 mm. The radius of the disk and the lenses are identical. The thickness of the disks and the thickness of the CCM section in the pCL lenses are kept the same at 2 mm.

The current density-voltage $(J - V)$ characteristics for the Alq$_3$ device are obtained with an HP-6634B DC power source controlled by a LabView program. The luminance is obtained through the transparent glass substrate with a Minolta CS-100 luminance meter. Device output power is recorded by Newport 1830-C optical power meter through an integrating sphere, and then calculated ($P_{\text{out}} = \int I(\lambda)/R(\lambda)d\lambda$) according to the responsivities of the power meter under the assumption that the electroluminescent (EL) spectrum is angle independent. $I(\lambda)$ and $R(\lambda)$ are the power meter photocurrent and detector responsivity for light incident at wavelengths between λ and $\lambda + d\lambda$. EL spectra were measured with an Ocean Optics SD 2000 fiber-optic spectrometer with the optical fiber attached above the OLED normal to the glass substrate. External quantum efficiency (η_{ext}) and luminous power efficiency (η_{lum}) are then calculated according to methods found in the literature [24].

III. EXPERIMENTAL RESULTS

A. *Engineering Highly Charge Balanced Device Structures*

Introduction: The energy level diagram of the OLED and the chemical structures of the corresponding materials are shown in Fig. 2. Values from the literature [15], [25]–[27] are used for the highest occupied molecular orbitals (HOMO) and the lowest unoccupied molecular orbitals (LUMO) of the organic materials and for the work function of the metal electrodes. ITO serves as the anode; PEDOT functions as a hole injection layer (HIL); PVK is a charge balance layer (CBL) whose purpose is to effectively slow down hole transport; and TPD or NPB are used as hole transport layers (HTL). It has been reported [28], [29] that devices fabricated with TPD or NPB showed similar device performance. TPD and NPB films have similar hole mobility [30] and only a slightly different HOMO/LUMO levels [25]. Therefore, devices fabricated with either TPD or NPB are comparable. Alq_3 is used for both the electron transport layer (ETL) and the emitter layer (EML); BCP functions as a hole blocking layer (HBL); LiF works as an efficient electron injection layer, and Al is used as the cathode.

A conventional bilayer OLED using Alq_3 as emitter usually has a structure of ITO/TPD/Alq_3/low-work-function cathode [7], [25], [31], [32]. This type of OLED generally produces an $\eta_{\text{ext}} \sim 1\%$, indicating a large potential for improvement of this structure. Since the energy barrier at the ITO/TPD interface is fairly large (~0.7 eV), a thin spin-coated layer of conductive polymer PEDOT is inserted to assist hole injection. PEDOT has a HOMO value of 5.2 eV, which is lower than the HOMO value of TPD but higher than the work function of ITO, so it can enhance hole injection [13]–[15] through stepwise injection from the anode. It was reported [33] that the hole mobility (10^{-3} $\mathrm{cm}^2/\mathrm{V}\cdot\mathrm{s}$) in the TPD or NPB film is 2 orders of magnitude higher than the electron mobility [34] (10^{-5} $\mathrm{cm}^2/\mathrm{V}\cdot\mathrm{s}$) in Alq_3, while the hole mobility [33] in PVK (10^{-5} $\mathrm{cm}^2/\mathrm{V}\cdot\mathrm{s}$) is quite comparable with the electron mobility in the Alq_3 layer. The incorporation of a PVK film in the device is expected to prevent holes from moving much faster than electrons, helping to balance e/h injection. The two polymer buffer layers, PEDOT and PVK are very important layers for high luminance and high efficiency device operation. Devices without any buffer layer are found to be inefficient and to degrade rapidly. There are many possible mechanisms for the improvement in performance achieved through the introduction of the polymer layers: reduction in the energy barrier between sequential layers [35], [36]; reduction in back-scattering of injected charges [37]; reduction in surface energy mismatch between the hydrophilic oxide anode and the hydrophobic arylamine HTL [13] which can cause poor physical adhesion.

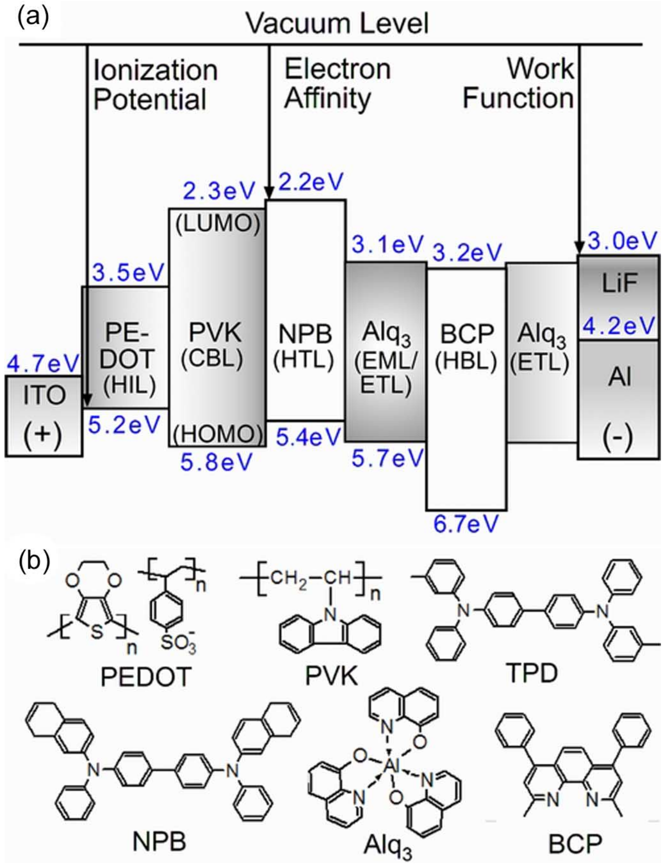

Fig. 2. Energy levels (a) and chemical structures (b) in the Alq_3 OLED with polymer layers and BCP layer. (Color version available online at http://ieeexplore.ieee.org.)

However, a device with the ITO/PEDOT/PVK/TPD/Alq_3/LiF:Al structure will still operate inefficiently at high current density (high luminance) because electrons have an energy barrier of 0.9 eV at the TPD/Alq_3 interface. This effectively confines electrons to the emitter layer. However, holes remain free to travel from the emitter layer toward the cathode where they will nonradiatively recombine. To prevent this, a BCP film is inserted into the device structure as a hole blocking layer. BCP has a HOMO value of 6.7 eV, which creates a 1.0-eV energy barrier for holes to escape the emitter layer. Furthermore, the BCP electron mobility is reported [38], [39] to be $\sim 10^{-4}$ $\mathrm{cm}^2/\mathrm{V}\cdot\mathrm{s}$, which is an order higher than that of Alq_3. Therefore, including a thin BCP HBL into the device will have only a minimum effect on the electron transport rate.

To determine the effect of different device structures design on device performance, five device types having the following structures were fabricated. Four devices of each type were measured. The spread in device characteristics was found to be <5%. ITO and LiF:Al were used as anode and cathode for all five devices:

A) PEDOT(50 nm)/TPD(60 nm)/Alq_3(40 nm);
B) PVK(50 nm)/TPD(60 nm)/Alq_3(40 nm);

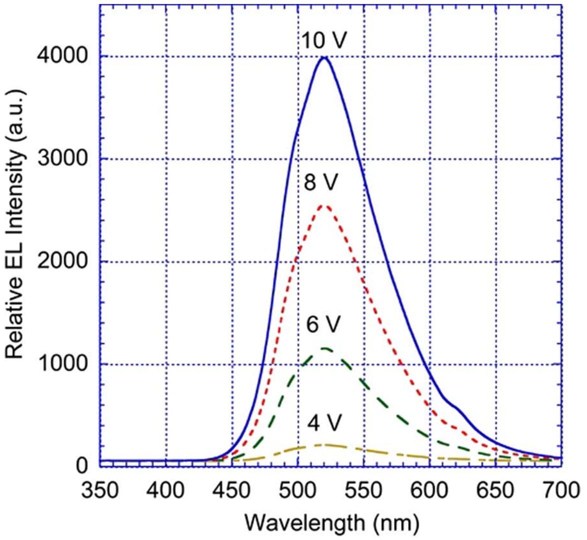

Fig. 3. Electroluminescent spectra of Alq$_3$ OLED at several bias voltages. (Color version available online at http://ieeexplore.ieee.org.)

C) PEDOT(50 nm)/NPB(30 nm)/Alq$_3$(40 nm)/BCP(20 nm)/Alq$_3$(10 nm);

D) PVK(50 nm)/NPB(30 nm)/Alq$_3$(40 nm)/BCP(20 nm)/Alq$_3$(10 nm);

E) PEDOT(50 nm)/PVK(50 nm)/NPB(30 nm)/Alq$_3$(40 nm)/BCP(20 nm)/Alq$_3$(10 nm).

Results and Discussion: Fig. 3 contains EL spectra of device A at operating voltages from 4 to 10 V. As expected in an Alq$_3$ device, the emission is in the green range, with a peak at 520 nm and full-width at half-maximum (FWHM) of 90 nm. The emission peak does not significantly shift with applied voltage. It was observed that the shape of EL spectra was identical in all five devices, with the difference only in the output power intensity at fixed operating voltage.

The luminance-current density-voltage (*L-J-V*) characteristics of devices A, B, C, D and E are shown in Fig. 4. Three-layer devices with different polymer layers of either PEDOT or PVK are compared in Fig. 4(a). The PEDOT buffered device (device A) turns on (defined as generating measurable optical emission of $\sim 0.01\ \mathrm{cd/m^2}$) at a bias of ~2.8 V, and reaches $300\ \mathrm{cd/m^2}$ at 6 V. The bias condition needed for reaching $300\ \mathrm{cd/m^2}$ luminance is a useful measure of comparison since that is the approximate level required for many display applications. The luminance saturates at a value of $\sim 10^4\ \mathrm{cd/m^2}$ at a bias of ~19 V. In comparison, device B with the PVK polymer layer turns on at a much higher voltage (7 V). This is consistent with its device structure: 1) in contrast to the highly conducting PEDOT, PVK is a semiconducting polymer and, therefore, including a 50 nm PVK layer into the device will introduce a significant voltage drop across this layer and 2) the ITO/PVK hole barrier of 1.1 eV in device B is much higher than the PEDOT/TPD hole barrier (0.2 eV). After turn on, the luminance of device B increases slowly with voltage, reaching $300\ \mathrm{cd/m^2}$ at a bias of 20 V. The luminance of device B saturates at a much lower value ($\sim 10^3\ \mathrm{cd/m^2}$) than device A at the higher voltage of 30 V.

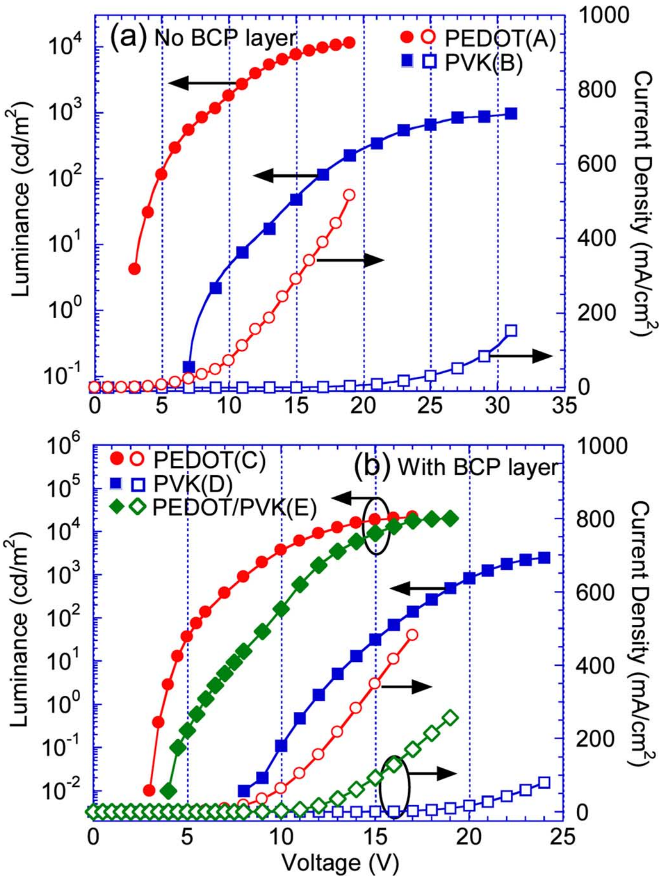

Fig. 4. Luminance and current density as a function of voltage. (a) Without BCP layer. (b) With BCP layer. (Color version available online at http://ieeexplore.ieee.org.)

Devices with the addition of the BCP HBL are compared in Fig. 4(b). Device C with the PEDOT polymer layer turns on at 3 V, which is nearly the same as device A. This is consistent with the organic layer thickness and the e/h energy barriers in these two device structures. After turn on, the luminance of device C increases rapidly with voltage, reaching $300\ \mathrm{cd/m^2}$ at 7 V and a saturation value of $\sim 2 \times 10^4\ \mathrm{cd/m^2}$ at a voltage of 16 V. The PVK buffered structure (device D) turns on at 8 V and can produce $300\ \mathrm{cd/m^2}$ at 18 V. The luminance saturates at a value $\sim 2500\ \mathrm{cd/m^2}$ at 24 V. Interestingly, the introduction of the HBL layer doubles the maximum luminance for both PEDOT and PVK devices. The device with dual polymer layers (device E) turns on at ~4 V, and reaches $300\ \mathrm{cd/m^2}$ at 11 V. The brightness saturates at about the same value ($\sim 2 \times 10^4\ \mathrm{cd/m^2}$) as device A, with a slightly higher bias of ~18 V but with only about half of the driving current.

Fig. 5 shows the luminous efficiency η_{lum} as a function of OLED luminance for the same five devices of Fig. 4. In general all five devices follow the same trend: a rapid increase in efficiency at low luminance levels, followed by a slow increase or a nearly constant efficiency over a wide range of luminance (approximately from one to three orders of magnitude), and finally a fairly sharp decrease at the highest luminance values. The external efficiencies of devices A and B reach their maximum value of ~0.85% (2.8 cd/A) and ~1.9% (6.4 cd/A) for luminance values of 5000 and $50\ \mathrm{cd/m^2}$, respectively. By comparison, devices C and D exhibit maximum efficiency values of ~1.8% (6 cd/A) and ~1.5% (5 cd/A), respectively. The saturated efficiency ranges for devices C and D are approximately

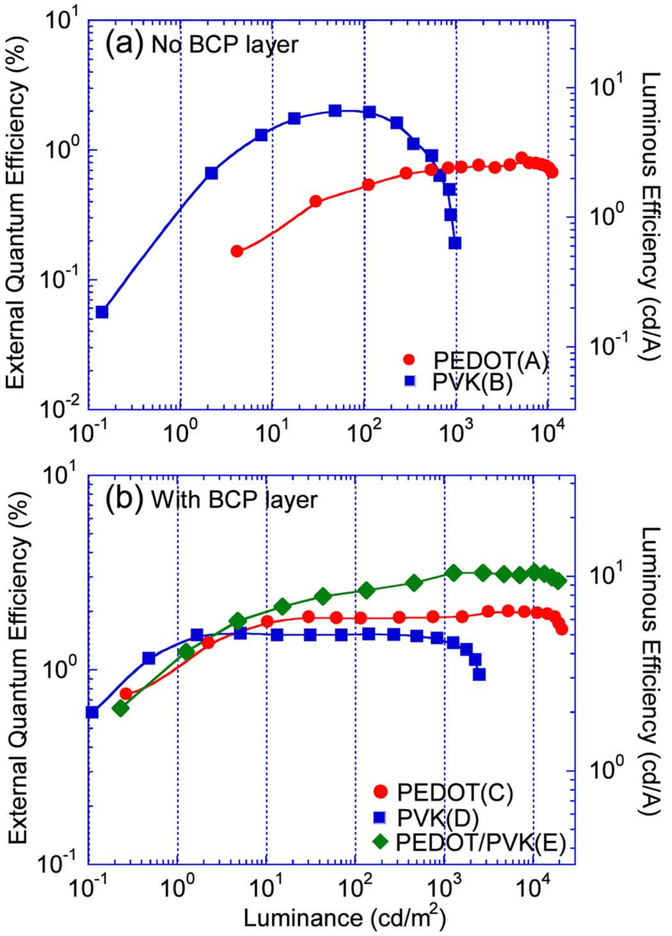

Fig. 5. External quantum and luminous efficiency for OLED structures with different polymer buffer layers and (a) without and (b) with BCP layer. (Color version available online at http://ieeexplore.ieee.org.)

from 10 to 15 000 $\mathrm{cd/m^2}$ and from 2 to 1000 $\mathrm{cd/m^2}$, respectively. Considering the charge transport mechanism in devices B and D, we can assume that their e/h charge transport rate is roughly the same, with the electron mobility through the Alq_3 layer matching the hole mobility through the PVK layer. However, because of the 1.1 eV ITO/PVK energy barrier, hole injection into the TPD (or NPB) layer is less efficient than electron injection into the Alq_3 emitting layer. This will result in electron build-up at the HTL/Alq_3 interface. Therefore, it is expected that most of the e/h recombination takes place at the HTL/Alq_3 interface and that it is rate-limited by hole injection. This supposition is supported by the fact that since similar efficiency values are obtained from these two devices, the incorporation of the HBL does not actually increase the maximum efficiency. Unlike devices B and D, devices A and C do not have a PVK layer to reduce the hole mobility. Therefore, holes will move much faster than electrons, resulting in excess holes at the TPD/Alq_3 (device A) or Alq_3/BCP (device C) interface. The recombination is then rate-limited by electron injection. In the case of device A, it is expected that holes can easily overcome the 0.3 eV energy barrier at the TPD/Alq_3 interface and move toward the cathode, resulting in a reduced efficiency value. Therefore, the incorporation of the HBL in device C is expected to confine the recombination to the Alq_3 layer by blocking the holes from further transporting to the cathode. The doubled efficiency value from device A to device C confirms this supposition. The external quantum efficiency η_{ext} of the dual polymer layer (device E) saturates at a value $>3\%$ (10 cd/A) for luminance values from 10^3 to over 10^4 $\mathrm{cd/m^2}$. The high efficiency of device E results from having both balanced e/h energy barriers and e/h mobilities. It is, therefore, likely that the e/h recombination occurs mostly within the Alq_3 layer.

B. *Lensed Approach to High Outcoupling Efficiency*

Introduction: The outcoupling efficiency, expressed as the ratio of surface emission intensity to total internal emission intensity, has been assumed to be less than 18% due to the critical angle of total internal reflection within the device [21]–[23]. The schematic diagrams in Fig. 1(c) and 1(d) illustrate the effect of the lens on the efficiency of the Alq_3 OLED. In the lensless device, the light reaching the glass–air interface at angles larger than the critical angle (θ_{c1}) is totally internally reflected and waveguided in the glass substrate. With the lens outcoupling technique, the light previously trapped in the glass substrate (within a cone from θ_{c1} to $\theta_{c2}, \theta_{c2} = \tan^{-1}(r/d)$) would now be emitted [parameters are defined in Fig. 1(d)].

Results and Discussion: Fig. 6 shows the output power density of lensed devices as a function of the driving current density. Hemispherical transparent lenses are incorporated with device E (dual polymer layer structure) to enhance the outcoupling efficiency. The epoxy lenses are 2.5 and 5 mm in radius with a refractive index of 1.56. For comparison, the performance of the same device without lens modification (lensless) is also shown. The device output power is dramatically enhanced by using the lensed structure. Compared to the lensless device, the output power is doubled for the 2.5-mm-lensed device and increases 2.5× for the 5-mm-lensed device. This is close to the maximum outcoupling enhancement factor [21]–[23] of ∼2.7 calculated by assuming that all the light previously waveguided in the glass substrate is now coupled out of the device. The maximum output power density is reached by the 5-mm-lensed device at 19 V (0.3 $\mathrm{A/cm^2}$), namely 45 $\mathrm{mW/cm^2}$ (calculated by using the 2×2 $\mathrm{mm^2}$ base size) compared to only 18 $\mathrm{mW/cm^2}$ for the lensless device. Fig. 1(e) and 1(f) show photographs taken under ambient lighting of the lensless device and of the 2.5-mm-lensed device operating at 6 V. Clearly, the power intensity of the 2.5-mm-lensed device is much higher than that of the lensless device. Fig. 1(g) and 1(h) illustrates the waveguiding effects in a lensless device and in a device with a 4-mm lens. The lensless device shows very bright edge emission, while edge emission from the 4-mm-lensed device has almost disappeared. Alternately, we estimate at least a doubling of OLED operational lifetime for the lensed devices under the same luminance condition, since they require only about one-half the input power of the lensless devices.

Efficiency (η_{ext} and η_{lum}) as a function of current density is shown in Fig. 7 for device E with various lens sizes. The 5-mm-lensed device has a maximum η_{ext} of ∼8%. This compares to the highest η_{ext} of 1.2%–1.4% reported [13], [31] for undoped Alq_3 lensless devices and 4–5% for doped Alq_3 lensless devices [27], [40]. The highest η_{lum} value of ∼7.5 lm/W is achieved with the same lensed device at $\sim$ 10 $\mathrm{mA/cm^2}$. Both η_{ext} and η_{lum} increase approximately 2.5× for the 5-mm-lensed

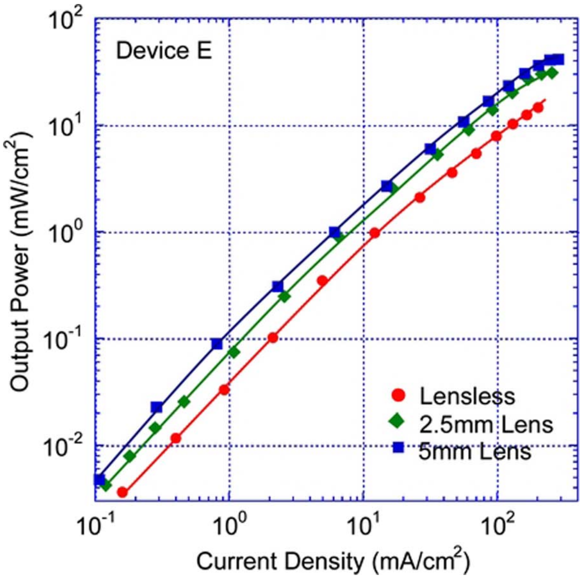

Fig. 6. Output power density as a function of OLED current density for lenses of various sizes. (Color version available online at http://ieeexplore.ieee.org.)

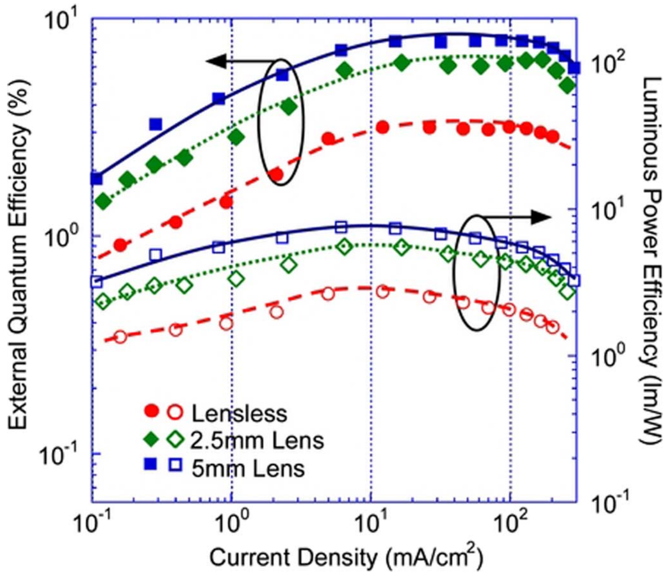

Fig. 7. OLED external quantum and luminous power efficiency as a function of current density for lenses of various sizes. (Color version available online at http://ieeexplore.ieee.org.)

device and 2.0× for the 2.5-mm-lensed device compared to the lensless device, which has its maximum η_{ext} and η_{lum} of ~3.2% and 2.8 lm/W, respectively. Remarkably, both η_{ext} and η_{lum} are constantly high (>2% and >2.5 lm/W, respectively) over the entire operating range from 0.1 mA/cm^2 to over 200 mA/cm^2 for the 5-mm-lensed device. This compares favorably to most phosphorescent devices, which have very high η_{ext} at low current, but experience a rapid drop in efficiency with increased driving current. The hybrid fluorescent device appears to be quite competitive for high luminance (high current) applications.

Fig. 8 shows the far-field power distribution of our devices. As shown in Fig. 8(a), the measured (individual data points) emission from the lensless device matches very well with the calculated Lambertian pattern (dashed lines). For the different lensed devices the measured far-field power distribution changes significantly from the lensless case. The power intensity increased much more in the direct viewing direction than at large viewing angles. The distribution pattern for lensed devices can be modified further by adjusting the height of the lens. Lenses with the same spherical radius of 5 mm were modified to vary the dome height from high ($h = 8$ mm), to medium ($h = 5$ mm) and low ($h = 3$ mm). As shown in Fig. 8(b), the far field power distribution changes dramatically with dome height. The low dome still resembles the Lambertian power distribution pattern, with a mostly even increase of the power intensity in all directions over the lensless device. The medium and high dome, however, increase the power output mostly in the direct viewing direction. Using the high dome, the power intensity in the surface normal direction increases more than 13× over the lensless device. This indicates the great potential of lensed OLEDs in the area of super bright output power concentrated in the direct viewing direction.

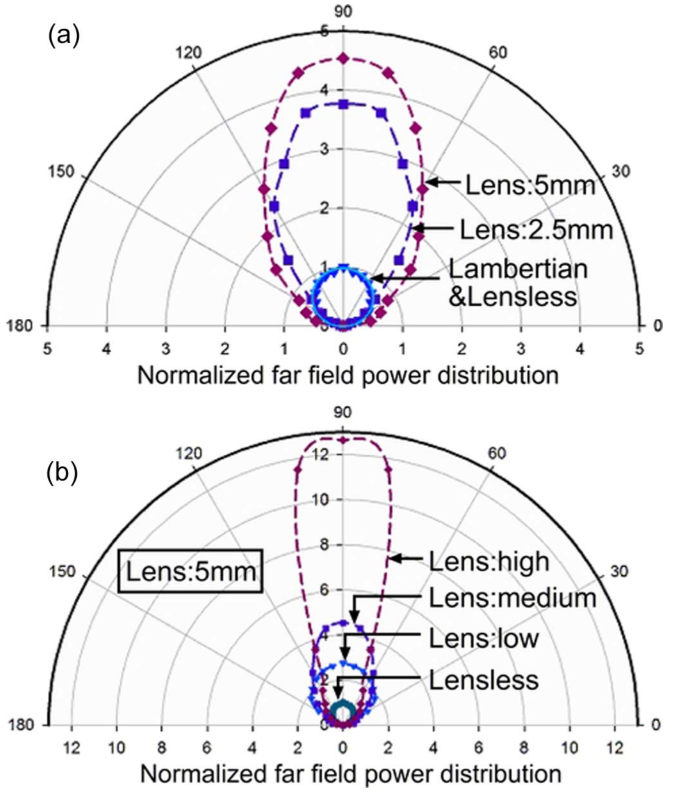

Fig. 8. Far-field output power distribution: (a) for lenses of different sizes and (b) for 5 mm lenses of different heights. (Color version available online at http://ieeexplore.ieee.org.)

C. *Lensed Approach to High Color Conversion Efficiency*

Introduction: Color down conversion is well known [3], [41] to be a very convenient and flexible method to achieve various colors. It is obtained by optically pumping an efficient color down conversion material (CCM), usually a planar thin film, frequently yielding an internal quantum efficiency (η_{int}) of >90%. The color conversion method though, has some potential problems to be overcome in both display application and lighting application if one uses planar CCMs to modify the glass side of the OLED device: 1) "color bleeding" due to the waveguiding light pumping adjacent pixels in display pixel arrays [42]; 2)

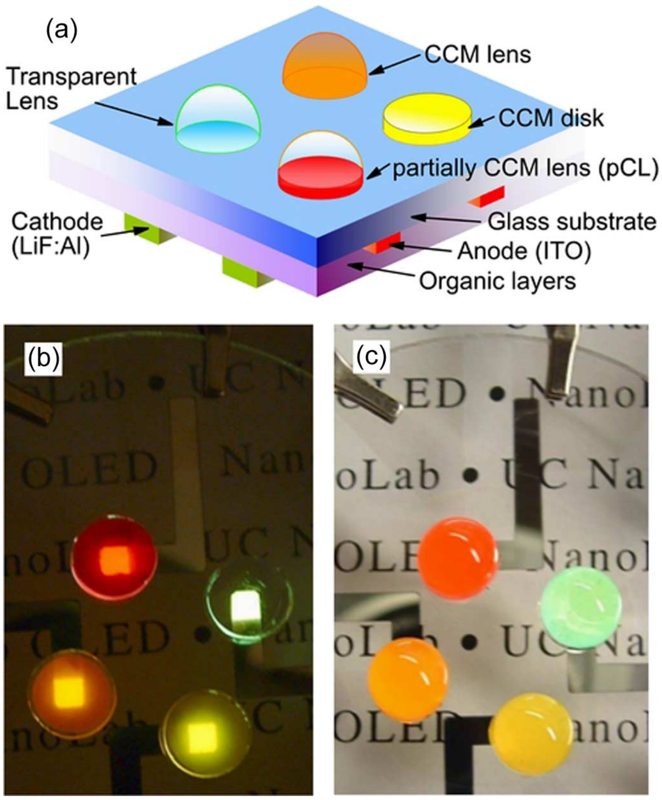

Fig. 9. High color conversion efficiency devices using lensed approach. (a) Schematic structure of the color conversion approach in $\mathrm{Alq_3}$ device. (b) Waveguiding effect for devices with CCM disk conversion operating at 5 V. (c) Emission from devices with partially CCM lens (pCL) operating at 5 V. (Color version available online at http://ieeexplore.ieee.org.)

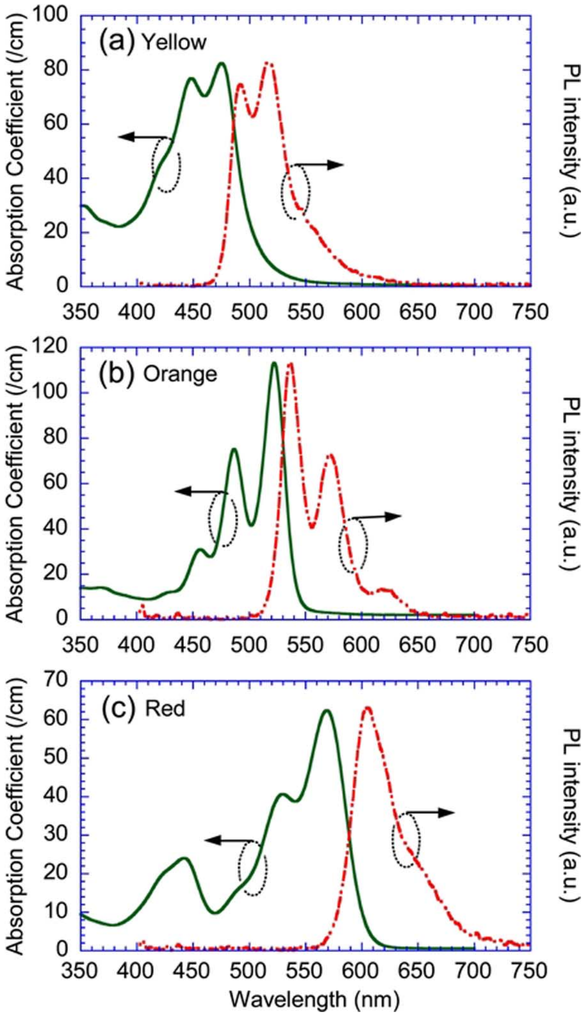

Fig. 10. Absorption coefficient of CCM films and their corresponding photoluminescent spectra. (a) CCM yellow. (b) CCM orange. (c) CCM red. (Color version available online at http://ieeexplore.ieee.org.)

absorbed light being reemitted isotropically and then mostly waveguided in the glass substrate and the CCM layers, causing significant loss of useful output power; and 3) back-emitted light being largely absorbed or waveguided and thus not available in the viewing direction. Therefore, the useful color conversion efficiency from a planar CCM is in practice less than 50%.

Results and Discussion: Fig. 9(a) shows a schematic diagram of an OLED 2 × 2 array with each device using a different outcoupling elements: transparent lens, CCM disk, CCM lens and partially CCM lens (pCL). Perylene-based lumophores are selected as dopants: yellow, orange, and red. Lumophores of this type have been reported [43] to have high quantum efficiency, long lifetime and stability under environmental stress conditions. The doping concentrations are 0.2 wt%, 0.1 wt%, and 0.05 wt% for yellow, orange, and red, respectively. Concentrations are selected to minimize the self-quenching and reabsorption but yet maintain true color. Fig. 9(b) shows a dark ambient photograph of the 2 × 2 OLED array in operation (at 5-V bias) with one transparent disk and three CCM disks. Fig. 9(c) shows the operation of the same array with three pCLs and one transparent (undoped) lens under normal ambient light. Green light originating from the $\mathrm{Alq_3}$ emitter passes through the glass substrate and is mostly absorbed by the CCM layers. Vivid yellow, orange and red colors are observed from the different pCL devices. In the case of the CCM disk array, the large difference of refractive index between the CCM layer $(n = 1.4)$ and air $(n = 1.0)$ will cause the isotropically reemitted luminescence in the forward direction to experience total internal reflection when the incident light angle exceeds the critical angle at the CCM–air interface. This will result in a total of ~70% of the reemitted light being totally reflected and waveguided in both the glass substrate and the CCM layer. Bright edge emission resulting from this waveguiding effect is clearly observed from the disks and glass substrate. In the pCL case, because much of the reemitted light in the forward direction is incident almost perpendicular to the lens/air interface, most of the luminescence reemitted in the viewing direction can now escape from the device. An exception to this is light originating at the edge of the lens can still experience waveguiding.

Fig. 10 shows the absorption coefficients and photoluminescence (PL) for the yellow, orange, and red CCMs. The absorption coefficients are obtained from the selected concentrations for the CCM films. To minimize reabsorption, the PL spectra are obtained by pumping very thin films of extremely dilute CCM solutions. Clearly, the absorption spectra of the various CCMs overlap with their emission spectra to a great extent. This can result in strong self-absorption and lead to a decrease of the color conversion efficiency. At the same time the emission spectra will become red-shifted as a result of self-absorption.

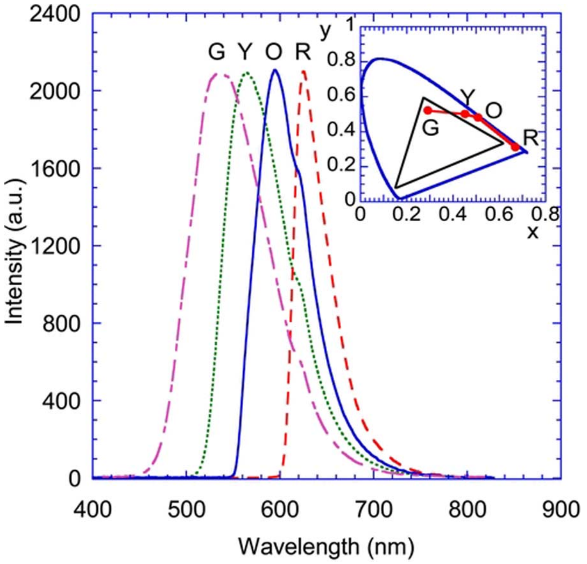

Fig. 11. EL spectra of green (G), yellow (Y), orange (O), and red (R) OLEDs. The green device uses a transparent lens; yellow, orange, and red devices use partially CCM lens (pCL). The insert shows the color coordinates of the four devices on the 1931 Commission Internationale de l'Eclairage (CIE) diagram. (Color version available online at http://ieeexplore.ieee.org.)

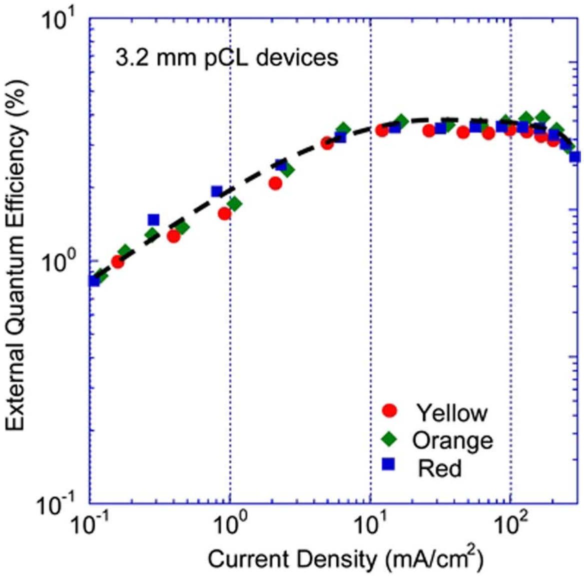

Fig. 12. OLED external quantum efficiency as a function of driving current for devices with partially CCM lenses (pCLs). (Color version available online at http://ieeexplore.ieee.org.)

Fig. 11 contains the EL spectra of the transparent-lensed green (G) device in addition to the yellow (Y), orange (O), and red (R) pCL devices. The insert in Fig. 11 shows the color coordinates of the four devices on the 1931 Commission Internationale de l'Eclairage (CIE) diagram. Clearly, the emission from the CCM-down-converted OLEDs shows saturated yellow, orange, and red colors. The EL emission spectra for the yellow, orange, and red devices exhibit red shifts from their corresponding PL spectra in Fig. 10. For the yellow device, the higher energy peak in its PL spectrum at 490 nm is not present in the OLED emission spectrum where pumping occurs at a longer wavelength. The lower energy peak of the yellow device at 515 nm is shifted to 565 nm. Similarly for the orange device, the first peak at 535 nm in the PL spectrum is not present in the EL spectrum, while the second peak has shifted from 553 to ~595 nm. Finally, the emission peak for the red device is shifted from 605 to ~620 nm. Devices outfitted with the CCM lenses experience a higher degree of spectrum red-shifting than the pCL devices because of the increased volume of CCM in the lens, resulting in decreased color conversion efficiency.

Fig. 12 shows the $\eta_{\rm ext}$ of the Y, O, and R pCL devices. In general, the $\eta_{\rm ext}$ of the three devices has the same dependence on driving current. The efficiency values increase rapidly at low current levels, followed by a nearly constant efficiency over a wide range of operating conditions (approximately from 5 to 200 mA/cm^2), and finally experience a rapid decline at the highest current levels. As a result of the enhancement in outcoupling efficiency provided by the lensed approach and high color conversion efficiency of the CCMs, the pCL devices have a higher $\eta_{\rm ext}$ than the original lensless device. The maximum $\eta_{\rm ext}$ can be as high as $\sim 4\%$ (compared to 3.2% for the original lensless device) for yellow, orange and red pCL devices and stays over 1% for almost entire driving current range from $0.1 \mathrm{mA/cm}^2$ to$>$ $200\ \mathrm{mA/cm}^2$.

IV. SUMMARY AND CONCLUSIONS

Bright, high power output hybrid Alq$_3$ OLEDs which incorporate index-matched hemispherical lenses for enhanced output power efficiency have been reported. Polymer (CBL) and small molecule (HBL) layers have been introduced to control the location of the recombination process. This hybrid polymer/small molecule structure provides more balanced charge injection, resulting in high luminance and efficiency and a more stable device over a large brightness range. Outcoupling efficiency enhancement as high as 2.5× has been obtained by using the lensed approach. The $\eta_{\rm lum}$ and $\eta_{\rm ext}$ can be as high as 7.5 lm/W and 8%, respectively, for the lensed device. These are the highest efficiency values reported for *undoped* Alq$_3$ devices. Using lensed color down conversion media, saturated yellow, orange and red devices with high conversion efficiency were demonstrated. An external quantum efficiency of $\sim 4\%$ is achieved for all three devices. In conclusion, the lensed approach is a very useful and flexible approach for improving the performance of OLEDs.

REFERENCES

[1] C. W. Tang and S. A. VanSlyke, "Organic electroluminescent diodes," *Appl. Phys. Lett.*, vol. 51, pp. 913–915, 1987.

[2] S. W. Wen, M. T. Lee, and C. H. Chen, "Recent development of blue fluorescent OLED materials and devices," *J. Disp. Technol.*, vol. 1, no. 1, pp. 90–99, Sep. 2005.

[3] A. J. Steckl, J. Heikenfeld, and S. C. Allen, "Light wave coupled flat panel displays and solid-state lighting using hybrid inorganic/organic materials," *J. Display Technol.*, vol. 1, no. 1, pp. 157–166, Sep. 2005.

[4] E. H-E. Wu, S.-H. Li, C.-W. Chen, G. Li, Z. Xu, and Y. Yang, "Controlling optical properties of electrodes with stacked metallic thin films for polymeric light-emitting diodes and displays," *J. Display Technol.*, vol. 1, no. 1, pp. 105–111, Sep. 2005.

[5] M. G. Mason, C. W. Tang, L. S. Hung, P. Raychaudhuri, J. Madathil, D. J. Giesen, L. Yan, Q. T. Le, Y. Gao, S. Y. Lee, L. S. Liao, L. F. Cheng, W. R. Salaneck, D. A. d. Santos, and J. L. Bredas, "Interfacial chemistry of Alq$_3$ and LiF with reactive metals," *J. Appl. Phys.*, vol. 89, pp. 2756–2765, 2001.

[6] G. E. Jabbour, M. M. Morrell, Y. Kawabe, B. Kippelen, N. Peyghambarian, M.-F. Nabor, R. Schlaf, E. A. Mash, and N. R. Armstrong, "Bright blue organic light-emitting diode with improved color purity using a LiF/Al cathode," *J. Appl. Phys.*, vol. 84, pp. 2324–2327, 1998.

[7] E. I. Haskal, A. Curioni, P. F. Seidler, and W. Andreoni, "Lithium-aluminum contacts for organic light-emitting devices," *Appl. Phys. Lett.*, vol. 71, pp. 1151–1153, 1997.

[8] X. Y. Deng, S. W. Tong, L. S. Hung, Y. Q. Mo, and Y. Cao, "Role of ultrathin Alq$_3$ and LiF layers in conjugated polymer light-emitting diodes," *Appl. Phys. Lett.*, vol. 82, pp. 3104–3106, 2003.

[9] Y. Yang and Q. Pei, "Electron injection polymer for polymer light-emitting diodes," *J. Appl. Phys.*, vol. 77, pp. 4807–4809, 1994.

[10] T. Kanbara, T. Yamamoto, K. Ishikawa, H. Takezoe, and A. Fukuda, "Polyquinoxaline as an excellent electron injecting material for electroluminescent device," *Appl. Phys. Lett.*, vol. 68, pp. 2346–2348, 1996.

[11] C. W. Tang, S. A. VanSlyke, and C. H. Chen, "Electroluminescence of doped organic thin films," *J. Appl. Phys.*, vol. 65, pp. 3610–3616, 1989.

[12] T. J. Marks, J. G. C. Veinot, J. Cui, H. Yan, A. Wang, N. L. Edleman, J. Ni, Q. Huang, P. Lee, and N. R. Armstrong, "Progress in high work function TCO OLED anode alternatives and OLED nanopixelation," *Synth. Met.*, vol. 127, pp. 29–35, 2002.

[13] J. Cui, Q. Huang, J. G. C. Veinot, H. Yan, and T. J. Marks, "Interfacial microstructure function in organic light-emitting diodes: assembled tetraaryldiamine and copper phthalocyanine," *Adv. Mater.*, vol. 14, pp. 565–569, 2002.

[14] S. Kim, D. Chung, J. Hong, T. Chung, T. Kim, W. Lee, and K. Jang, "Effects of buffer layer in organic light-emitting diodes," *Mol. Cryst. Liq. Cryst.*, vol. 377, pp. 129–132, 2002.

[15] T. Kugler and W. R. Salaneck, "Characterization of the PEDOT-PSS system by means of X-ray and ultraviolet photoelectron spectroscopy," *Thin Solid Films*, vol. 354, pp. 129–135, 1999.

[16] J. R. Sheats, H. Antoniadis, M. Heuschen, W. Leonard, J. Miller, R. Moon, D. Roitman, and A. Shocking, "Organic electroluminescent devices," *Science*, vol. 273, pp. 884–887, 1996.

[17] V. Bulovic, V. B. Khalfin, G. Gu, P. E. Burrows, D. Z. Garbuzov, and S. R. Forrest, "Weak microcavity effects in organic light-emitting devices," *Phys. Rev. B*, vol. 58, pp. 3730–3740, 1998.

[18] S. Wang, Y. Q. Liu, X. B. Huang, S. L. Xu, J. R. Gong, X. H. Chen, L. Yi, Y. Xu, G. Yu, L. J. Wan, C. L. Bai, and D. B. Zhu, "Organic light-emitting diodes with improved hole-electron balance by using molecular layers of phthalocyanine to modify the anode surface," *Appl. Phys. A*, vol. 78, pp. 553–556, 2004.

[19] N. C. Greenham, R. H. Friend, and D. D. C. Bradley, "Angular dependence of the emission from a conjugated polymer light-emitting diode: implications for efficiency calculations," *Adv. Mater.*, vol. 6, pp. 491–494, 1994.

[20] T. Yamasaki, K. Sumioka, and T. Tsutsui, "Organic light-emitting device with an ordered monolayer of silica microspheres as a scattering medium," *Appl. Phys. Lett.*, vol. 76, pp. 1243–1245, 2000.

[21] G. Gu, D. Z. Garbuzov, P. E. Burrows, S. Venkatesh, and S. R. Forrest, "High-external-quantum-efficiency organic light-emitting devices," *Opt. Lett.*, vol. 22, pp. 396–398, 1997.

[22] T. Tsutsui, M. Yahiro, H. Yokogawa, K. Kawano, and M. Yokoyama, "Doubling coupling-out efficiency in organic light-emitting devices using a thin silica aerogel layer," *Adv. Mater.*, vol. 13, pp. 1149–1152, 2001.

[23] C. F. Madigan, M. H. Lu, and J. C. Sturm, "Improvement of output coupling efficiency of organic light-emitting diodes by backside substrate modification," *Appl. Phys. Lett.*, vol. 76, pp. 1650–1652, 2000.

[24] S. R. Forrest, D. D. C. Bradley, and M. E. Thompson, "Measuring the efficiency of organic light-emitting devices," *Adv. Mater.*, vol. 15, pp. 1043–1048, 2003.

[25] T. Mori, T. Ogawa, D. Cho, and T. Mizutani, "A discussion of conduction in organic light-emitting diodes," *Appl. Surf. Sci.*, vol. 212–213, pp. 458–463, 2003.

[26] M. A. Baldo, M. E. Thompson, and S. R. Forrest, "Phosphorescent materials for application to organic light emitting devices," *Pure Appl. Chem.*, vol. 71, pp. 2095–2106, 1999.

[27] Q. Huang, J. Cui, J. G. C. Veinot, H. Yan, and T. J. Marks, "Realization of high-efficiency/high-luminance small-molecule organic light-emitting diodes: synergistic effects of siloxane anode functionalization/hole-injection layers, and hole/exciton-blocking/electron-transport," *Appl. Phys. Lett.*, vol. 82, pp. 331–333, 2003.

[28] D. F. O'Brien, P. E. Burrows, S. R. Forrest, B. E. Koene, D. E. Loy, and M. E. Thompson, "Hole transporting materials with high glass transition temperatures for use in organic light-emitting devices," *Adv. Mater.*, vol. 10, pp. 1108–1112, 1998.

[29] H. Fujikawa, M. Ishii, S. Tokito, and Y. Taga, "Organic light-emitting diodes using triphenylamine based hole transporting materials," in *Proc. Mat. Res. Soc. Symp.*, 2000, vol. 621.

[30] S. Naka, H. Okada, H. Onnagawa, Y. Yamaguchi, and T. Tsutsui, "Carrier transport properties of organic materials for EL device operation," *Synth. Met.*, vol. 111–112, pp. 331–333, 2000.

[31] P. E. Burrows, Z. Shen, V. Bulovic, D. M. McCarty, S. R. Forrest, J. A. Cronin, and M. E. Thompson, "Relationship between electroluminescence and current transport in organic heterojunction light-emitting devices," *J. Appl. Phys.*, vol. 79, pp. 7991–8006, 1996.

[32] S. R. Forrest, "Ultrathin organic films grown by organic molecular beam deposition and related techniques," *Chem. Rev*, vol. 97, pp. 1793–1896, 1997.

[33] G. E. Johnson, K. M. McGrane, and M. Stolka, "Electroluminescence from single layer molecularly doped polymer films," *Pure Appl. Chem.*, vol. 67, pp. 175–182, 1995.

[34] B. J. Chen, W. Y. Lai, Z. Q. Gao, C. S. Lee, S. T. Lee, and W. A. Gambling, "Electron drift mobility and electroluminescent efficiency of tris(8-hydroxyquinolinolato) aluminum," *Appl. Phys. Lett.*, vol. 75, pp. 4010–4012, 1999.

[35] S. T. Lee, Y. M. Wang, and X. Y. Houb, "Interfacial electronic structures in an organic light-emitting diode," *Appl. Phys. Lett.*, vol. 74, pp. 670–672, 1999.

[36] K. Book, H. Bassler, A. Elschner, and S. Kirchmeyer, "Hole injection from an ITO/PEDT anode into the hole transporting layer of an OLED probed by bias induced absorption," *Org. Electron.*, vol. 4, pp. 227–232, 2003.

[37] L. A Zuppiroli, L. Si-Ahmed, K. Kamaras, F. Nuesch, M. N. Bussac, D. Ades, A. Siove, E. Moons, and M. Gratzel, "Self-assembled monolayers as interfaces for organic opto-electronic devices," *Eur. Phys. J. B*, vol. 11, pp. 505–512, 1999.

[38] G. Parthasarathy, C. Shen, A. Kahn, and S. R. Forrest, "Lithium doping of semiconducting organic charge transport materials," *J. Appl. Phys.*, vol. 89, pp. 4986–4992, 2001.

[39] S. Naka, H. Okada, H. Onnagawa, and T. Tsutsui, "High electron mobility in bathophenanthroline," *Appl. Phys. Lett.*, vol. 76, pp. 197–199, 2000.

[40] M. A. Baldo, D. F. O'Brien, Y. You, A. Shoustikov, S. Sibley, M. E. Thompson, and S. R. Forrest, "Highly efficient phosphorescent emission from organic electroluminescent devices," *Nature*, vol. 395, pp. 151–154, 1998.

[41] A. R. Duggal, J. J. Shiang, C. M. Heller, and D. F. Foust, "Organic light-emitting devices for illumination quality white light," *Appl. Phys. Lett.*, vol. 80, pp. 3470–3472, 2002.

[42] P. E. Burrows, G. Gu, V. Bulovic, Z. Shen, S. R. Forrest, and M. E. Thompson, "Achieving full-color organic light-emitting devices for lightweight, flat-panel displays," *IEEE Trans. Electron Devices*, vol. 44, no. 8, pp. 1188–1203, Aug. 1997.

[43] G. Seybold and G. Wagenblast, "New perylene and violanthrone dyestuffs for fluorescent collectors," *Dyes and Pigments*, vol. 11, pp. 303–317, 1989.

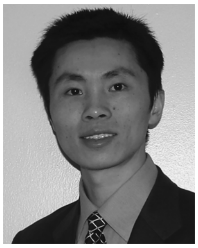

Weixin Li (S'05) received the B.S. degree (with high honors) in material science from Shanghai University, Shanghai, China, in 1997, and began his graduate program in 1999 in the same department, working on high permittivity, low loss microwave dielectric materials. He is currently working toward the PhD degree at the Nanoelectronics Laboratory in electrical engineering at the University of Cincinnati, Cincinnati, OH, focusing on full-color, high efficiency organic light emitting diodes (OLEDs).

His current area of interest is high efficiency organic-lanthanide doped OLEDs for display application.

Mr. Li is a student member of the American Physical Society, and the Society for Information Display.

Robert A. Jones (S'02) received the B.S. degree from the University of South Florida, Tampa, in 1998, and the M.S. degree in Physics from The University of Cincinnati, Cincinnati, OH, in 2001, all in physics. His Bachelors work focused on thin film growth by dual laser ablation for solar cell applications and his Masters work focused on the optical properties of CdSe self assembled quantum dots.

In 2001, he joined the Nanoelectronics Laboratory at the University of Cincinnati. As a research associate, he has worked in the area of GaN:RE phosphors grown by MBE for applications in thick dielectric electroluminescent flat panel displays. As a Ph.D.

candidate, his current area of interest is UHV and hybrid deposition and fabrication of organic materials for display, laser and optical communications applications. He has presented several formal presentations, including the national meetings of the American Physical Society and the Society of Information Display.

Mr. Jones is a member of the Institute of Electrical and Electronics Engineers, Inc., the American Physical Society, Sigma Pi Sigma Physics Honor Society, the Society for Information Display, and the Materials Research Society.

Steven C. Allen (S'05) received the B.S. degrees in physics and chemistry at Ohio University, Athens, in 2001, and the M.S.E. degree in electrical engineering from Princeton University, Princeton, NJ, in 2003. He is currently working toward the Ph.D. degree in electrical engineering at the University of Cincinnati, Cincinnati, OH. In his doctoral study he is focusing on novel lamp designs for solid state lighting applications.

Jason C. Heikenfeld (S'99–M'01) received the B.S. and Ph.D. degrees in electrical engineering with minors in both photonics and physics from the University of Cincinnati, Cincinnati, OH, in 1998 and 2001, respectively.

During 2001–2005, he was principal scientist and a co-founder at Extreme Photonix Corporation. In 2005 he returned to the University of Cincinnati as an Assistant Professor in the Department of Electrical and Computer Engineering and Computer Science. His university laboratory, The Novel Devices Laboratory, http\\:www.ececs.uc.edu/devices, is currently engaged in multi-disciplinary research paths spanning photonics, nanoscale structures, electrowetting, and biological devices. He has authored and coauthored over 100 publications in refereed journals, industry magazines, conference proceedings, and a book chapter. He is an inventor of both granted and several pending U.S. patents. He is a member of the IEEE Lasers and Electro-Optics Society and the Society for Information Display.

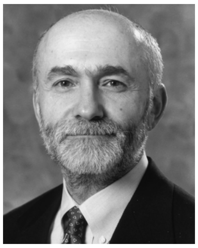

Andrew J. Steckl (S'70–M'73–SM'79–F'99) received the B.S.E. degree in electrical engineering from Princeton University, Princeton, NJ, in 1968, and the M.Sc. and Ph.D. Degrees from the University of Rochester, Rochester, NY, in 1970 and 1973, respectively.

In 1972, Dr. Steckl joined the Honeywell Radiation Center, Lexington, MA, as a Senior Research Engineer, where he worked on new concepts and devices in the area of infrared detection. In 1973, he joined the Technical Staff of the Electronics Research Division of Rockwell International, Anaheim, CA. At Rockwell he was primarily involved in research on charge coupled devices. In 1976, he joined the Electrical, Computer and Systems Engineering Department at Rensselaer Polytechnic Institute, Troy, NY, where he developed a research program in microfabrication of Si devices. In 1981, he founded the Center for Integrated Electronics, a multi-disciplinary academic center focused on VLSI research and teaching, and served as its director until 1986. In 1988, he joined the Electrical and Computer Engineering Department of the University of Cincinnati as Ohio Eminent Scholar and Gieringer Professor of Solid State Microelectronics. At Cincinnati, he has built the Nanoelectronics Laboratory in the general area of semiconductor materials and devices for photonics. Current activities include GaN MBE growth, rare-earth-doped organic and inorganic luminescent devices, hybrid inorganic/organic materials and devices for flat panel displays and solid-state lighting. His research has resulted in over 340 publications and over 350 conference and seminar presentations.